Title
Escape forces and trajectories in optical tweezers and their effect on calibration

Journal
Optics Express, 23(19)

ISSN
1094-4087

Authors
Bui, Ann AM
Stilgoe, Alexander B
Khatibzadeh, Nima
et al.

Publication Date
2015-09-21

DOI
10.1364/oe.23.024317

Escape forces and trajectories in optical tweezers and their effect on calibration

Ann A. M. Bui,[1,*] Alexander B. Stilgoe,[1] Nima Khatibzadeh,[2] Timo A. Nieminen,[1] Michael W. Berns,[2,3] and Halina Rubinsztein-Dunlop[1]

[1]*School of Mathematics and Physics, The University of Queensland, St. Lucia, QLD, 4072, Australia*

[2]*Beckman Laser Institute and Medical Clinic, University of California, Irvine, CA, 92612, USA*

[3]*Institute of Engineering in Medicine, University of California, San Diego, CA, 92093, USA*

[*]*a.bui@uq.edu.au*

Abstract: Whether or not an external force can make a trapped particle escape from optical tweezers can be used to measure optical forces. Combined with the linear dependence of optical forces on trapping power, a quantitative measurement of the force can be obtained. For this measurement, the particle is at the edge of the trap, away from the region near the equilbrium position where the trap can be described as a linear spring. This method provides the ability to measure higher forces for the same beam power, compared with using the linear region of the trap, with lower risk of optical damage to trapped specimens. Calibration is typically performed by using an increasing fluid flow to exert an increasing force on a trapped particle until it escapes. In this calibration technique, the particle is usually assumed to escape along a straight line in the direction of fluid-flow. Here, we show that the particle instead follows a curved trajectory, which depends on the rate of application of the force (i.e., the acceleration of the fluid flow). In the limit of very low acceleration, the particle follows the surface of zero axial optical force during the escape. The force required to produce escape depends on the trajectory, and hence the acceleration. This can result in variations in the escape force of a factor of two. This can have a major impact on calibration to determine the escape force efficiency. Even when calibration measurements are all performed in the low acceleration regime, variations in the escape force efficiency of 20% or more can still occur. We present computational simulations using generalized Lorenz–Mie theory and experimental measurements to show how the escape force efficiency depends on rate of increase of force and trapping power, and discuss the impact on calibration.

OCIS codes: (140.7010) Laser trapping; (350.4855) Optical tweezers or optical manipulation.

References and links

1. A. Ashkin, J. M. Dziedzic, J. E. Bjorkholm, and S. Chu, "Observation of a single-beam gradient force optical trap for dielectric particles," Opt. Lett. **11**, 288–290 (1986).
2. J. R. Moffitt, Y. R. Chemla, S. B. Smith, and C. Bustamante, "Recent advances in optical tweezers," Annu. Rev. Biochem. **77**, 205–228 (2008).
3. A. Farré, F. Marsà, and M. Montes-Usategui, "Optimized back-focal-plane interferometry directly measures forces of optically trapped particles," Opt. Express **20**, 12270–12291 (2012).

#246249 Received 21 Jul 2015; revised 28 Aug 2015; accepted 30 Aug 2015; published 8 Sep 2015

4. K. Svoboda and S. M. Block, "Biological applications of optical forces," Annu. Rev. Biophys. Biomol. Struct. **23**, 247–285 (1994).
5. W. M. Lee, P. J. Reece, R. F. Marchington, N. K. Metzger, and K. Dholakia, "Construction and calibration of an optical trap on a fluorescence optical microscope," Nat. Protoc. **2**, 3226–3238 (2007).
6. A. van der Horst and N. R. Forde, "Power spectral analysis for optical trap stiffness calibration from high-speed camera position detection with limited bandwidth," Opt. Express **18**, 7670–7677 (2010).
7. Y. Jun, S. K. Tripathy, B. R. J. Narayanareddy, M. K. Mattson-Hoss, and S. P. Gross, "Calibration of optical tweezers for in vivo force measurements: How do different approaches compare?" Biophys. J. **107**, 1474–1484 (2014).
8. H. Felgner, O. Müller, and M. Schliwa, "Calibration of light forces in optical tweezers," Appl. Opt. **34**, 977–982 (1995).
9. N. Khatibzadeh, A. B. Stilgoe, A. A. M. Bui, Y. Rocha, G. Cruz, T. A. Nieminen, H. Rubinsztein-Dunlop, and M. W. Berns, "Optical trapping of isolated mammalian chromosomes," Proc. SPIE **9164**, 91642I (2014).
10. N. Khatibzadeh, A. B. Stilgoe, A. A. M. Bui, Y. Rocha, G. M. Cruz, V. Loke, L. Z. Shi, T. A. Nieminen, H. Rubinsztein-Dunlop, and M. W. Berns, "Determination of motility forces on isolated chromosomes with laser tweezers," Sci. Rep. **4**, 6866 (2014).
11. A. A. M. Bui, A. B. Stilgoe, N. Khatibzadeh, T. A. Nieminen, H. Rubinsztein-Dunlop, and M. W. Berns, "Optical tweezers escape forces," Proc. SPIE **9164**, 916413 (2014).
12. A. B. Stilgoe, T. A. Nieminen, G. Knöner, N. R. Heckenberg, and H. Rubinsztein-Dunlop, "The effect of Mie resonances on trapping in optical tweezers," Opt. Express **16**, 15039–15051 (2008).
13. F. Merenda, G. Boer, J. Rohner, G. Delacrétaz, and R.-P. Salathé, "Escape trajectories of single-beam optically trapped micro-particles in a transverse fluid flow," Opt. Express **14**, 1685–1699 (2006).
14. Z. Gong, Z. Wang, Y. Li, L. Lou, and S. Xu, "Axial deviation of an optically trapped particle in trapping force calibration using the drag force method," Opt. Commun. **273**, 37–42 (2007).
15. Y. Cao, A. B. Stilgoe, L. Chen, T. A. Nieminen, and H. Rubinsztein-Dunlop, "Equilibrium orientations and positions of non-spherical particles in optical traps," Opt. Express **20**, 12987–12996 (2012).
16. A. A. M. Bui, A. B. Stilgoe, T. A. Nieminen, and H. Rubinsztein-Dunlop, "Calibration of nonspherical particles in optical tweezers using only position measurement," Opt. Lett. **38**, 1244–1246 (2013).
17. G. Volpe and G. Volpe, "Simulation of a Brownian particle in an optical trap," Am. J. Phys. **81**, 224–230 (2013).
18. H. Faxén, "Der Widerstand gegen die Bewegung einer starren Kugel in einer zähen Flüssigkeit, die zwischen zwei parallelen ebenen Wänden eingeschlossen ist," Ann. Phys. **373**, 89–119 (1922).
19. M. Chaoui and F. Feuillebois, "Creeping flow around a sphere in a shear flow close to a wall," Q. J. Mech. Appl. Math. **56**, 381–410 (2003).
20. T. A. Nieminen, V. L. Y. Loke, A. B. Stilgoe, G. Knöner, A. M. Brańczyk, N. R. Heckenberg, and H. Rubinsztein-Dunlop, "Optical tweezers computational toolbox," J. Opt. A **9**, S196–S203 (2007).
21. E. L. Botvinick and M. W. Berns, "Internet-based robotic laser scissors and tweezers microscopy," Microsc. Res. Techniq. **68**, 65–74 (2005).
22. G. Thalhammer, L. Obmascher, and M. Ritsch-Marte, "Direct measurement of axial optical forces," Opt. Express **23**, 6112-6129 (2015).

1. Introduction

Since the development of optical tweezers [1], there has been widespread application of non-contact trapping and manipulation in biology and other fields. Beyond this, they offer the opportunity to quantitatively measure forces on the order of piconewtons on a microscopic scale [2], and have proven to be a valuable tool in a broad range of experimental biophysics applications. In the typical mode of operation, the force is determined by either measuring the position of the particle within the trap using a camera, or by measuring the deflection of the forward scattered (i.e., transmitted) light using a quadrant photodiode (QPD) or position sensitive detector (PSD) [3]. In either case, it is necessary to calibrate the trap. If the particle remains close enough to the equilibrium position in the trap (region A of the force–position curve in Fig. 1), the trap can be treated as a Hookean (i.e., linear) spring. In this case, the calibration consists of determining the spring constant of the trap, and it is not necessary to determine the entire force–position curve. Various well-established methods are available for this task [4–7]. This ease of calibration is a major factor in the popularity of restricting force measurements to the linear region of the trap.

However, this is not the only mode in which forces can be measured with optical tweezers.

#246249 Received 21 Jul 2015; revised 28 Aug 2015; accepted 30 Aug 2015; published 8 Sep 2015

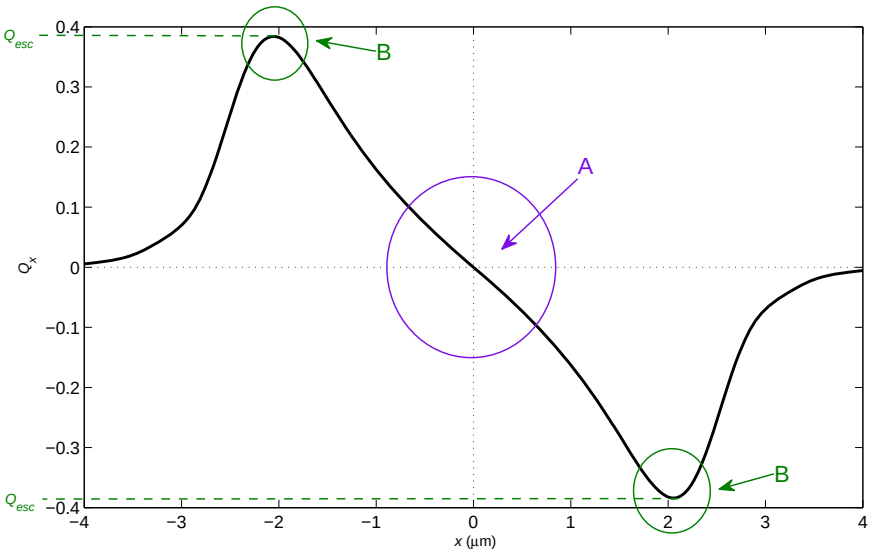

Fig. 1. Simulation showing regions of the force–position curve commonly used for force measurement with optical tweezers. The most common choice is the linear region A near the equilbrium, where the trap is approximately a Hookean spring. The maximum radial force region B allows higher forces to be measured for the same beam power, and at the same time reducing the risk of optical damage to live specimens.

It is also possible to use the maximum force portion of the force–position curve (region B in Fig. 1). This maximum force is the radial trap strength, and (radial) escape from the trap indicates that the forces exceed the trap strength. We can describe the linear relationship between the optical force **F** and the power of the trapping beam by introducing the dimensionless force efficiency **Q**, where

$$\mathbf{F} = \frac{n\mathbf{Q}}{c}P, \tag{1}$$

where P is the beam power at the trap and n is the refractive index of the surrounding medium, and c is the speed of light in free space. This **Q** is dimensionless and scales linearly with power. Since this relationship also applies to the trap strength, the magnitude of the radial force required to escape (radially) from the trap, F_{esc}, is

$$F_{\mathrm{esc}} = \frac{nQ_{\mathrm{esc}}}{c}P. \tag{2}$$

For escape force measurements of this type, calibration consists of finding Q_{esc}, which is typically done by using fluid flow to exert an increasing force on the particle until the particle escapes [8]. By varying the power, the minimum power required to keep the particle within the trap gives a quantitative measurement of the force. One advantage of this mode of force measurement is that much larger forces can be measured for the same beam power, compared with using the linear region of the trap, and at the same time reducing the likelihood of optical damage to live specimens.

Since the optical force is proportional to the beam power, we expect to obtain a linear relationship between the the spring constant or the escape force and the power if we calibrate the trap for different beam powers, as can be inferred from Eq. (2). That is, we expect to obtain

#246249 Received 21 Jul 2015; revised 28 Aug 2015; accepted 30 Aug 2015; published 8 Sep 2015

a constant Q_{esc}, independent of the power. A series of escape force calibration measurements were performed for spheres for the validation of an escape force calibration that was done for trapped isolated mammalian chromosomes [9, 10]. The results showed, contrary to the power independence hypothesis of Q_{esc}, a clear dependence on the power [11].

In a three dimensional optical trap, the axial component of the optical force has a zero force (stable trapping) surface; due to the change in relative back-scattering of light it must also be curved [12]. If a particle moves radially, it will also move axially due to a reduction in gradient force relative to the scattering force. Thus the escape of such particles cannot be along a straight-line purely radial trajectory—displacements in one axis cause displacements in another. The rate at which the external force which moves the particle away from the beam axis is applied is a key factor determining the trajectory; this is shown in Fig. 2. If the force is applied slowly, the trajectory of the particle closely follows the zero-force surface (the black curve maked "Slow", and the white region behind it and mirroring it on the left, in Fig. 2). If the force is applied rapidly, the trajectory will be close to a straight line in the direction of the applied force. Between these limits, the particle will escape on a trajectory lying between these extremes.

Since the optical force is a complicated three-dimensional function of position within the trap, the particle experiences different optical forces along these different trajectories. Therefore, the forces required to produce escape along different trajectories will vary. Such variations in the escape force have been seen previously [13, 14]. Considering the different forces seen along these extreme trajectories, we might expect a variation of a factor of two, with direct horizontal escape (i.e., rapidly applied escape force) resulting in doubling of the escape force compared with slowly applied forces. We present computational simulations using generalized Lorenz–Mie theory and experimental measurements to show how the escape force efficiency depends on rate of increase of force and trapping power, and discuss the impact on calibration. Notably, even if calibration and measurement are all performed in the low rate of increase of force, low escape force efficiency regime, variations in the escape force efficiency of 20% or more can still occur.

2. Simulations

The goal of our simulations is to model the escape of particles from a trap due to a viscous drag force that changes in time. This models the escape force calibration of an optical trap using a stage undergoing constant acceleration to provide the escape force, through associated motion of the fluid surrounding the particle. The fluid is assumed to move together with the stage, with the same instantaneous velocity. Simulations allow us to explore the behaviour of the system over a wide range of parameters, including values inaccessible through available experimental apparatus. In addition, the optical forces in the simulated trap are known *a priori*, allowing comparison of the simulated calibration results and the optical forces. To simulate the motion of the particle within the trap, we solve Langevin's equation using Euler's method [15–17], with a time-varying escape force.

The escape of a trapped particle can be simulated by considering the effect of a force acting on the particle. At the low Reynolds numbers encountered in optical tweezers, the velocity of a sphere moving through a fluid is such that the driving force $\mathbf{f}_{\text{flow}}$ is in equilibrium with the viscous drag force, such that

$$\mathbf{f}_{\text{flow}} = \Gamma\mathbf{v} = 6\pi\eta r\mathbf{v}, \tag{3}$$

where η is the (temperature dependent) viscosity of a classical Newtonian fluid (such as water), r is the radius of the particle and $\mathbf{v}$ is the velocity of the stage, which creates the fluid flow. Here, we have made the substitution $\Gamma = 6\pi\eta r$, but in general, Γ is a tensor. For chiral objects this tensor will also couple rotational to translational degrees of freedom. Here, we will deal with just the spherical case, but the outlined simulation method can be applied to more general

#246249 Received 21 Jul 2015; revised 28 Aug 2015; accepted 30 Aug 2015; published 8 Sep 2015

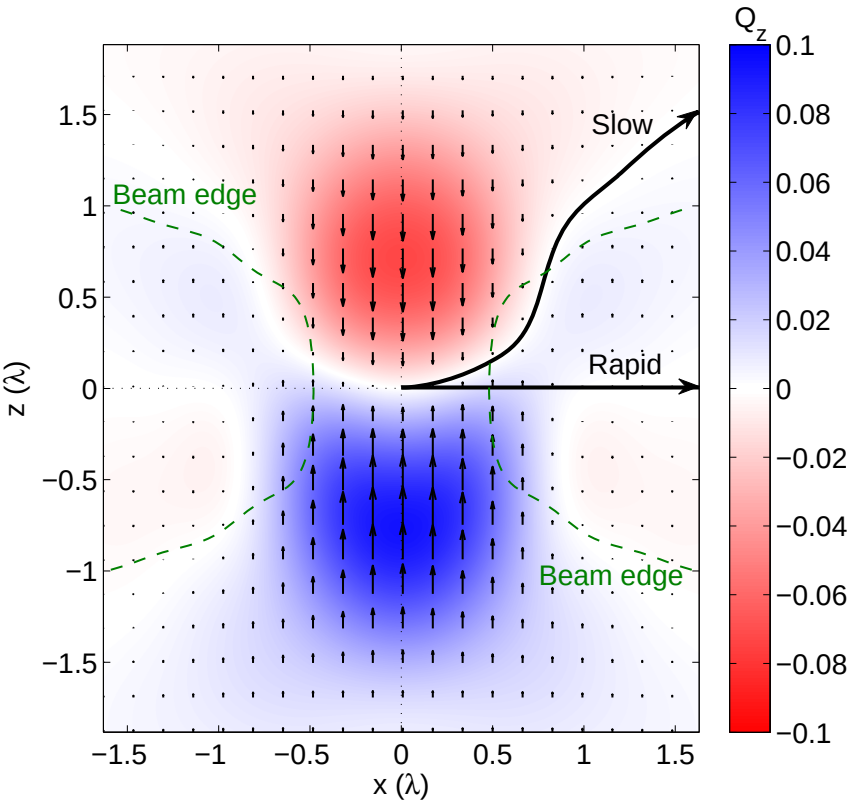

Fig. 2. Simulation showing that escape trajectories depend on the rate at which the force causing escape is applied. Extreme escape trajectories are shown for an optical trap, with the trapping beam propagating vertically upwards, and escape force applied horizontally to the right. The colour map shows the axial forces of the optical trap. One extreme case is a very rapid application of the escape force, when the particle escapes from the trap before the optical forces have time to move the particle significantly in the vertical direction. In this case, the escape trajectory is a horizontal straight line. The other extreme case is very slow application of the escape force, when the particle will follow a trajectory such that the vertical (i.e., axial) optical forces is zero. In this case, the trajectory lies on the (mathematical) surface where the vertical optical forces are in equilibrium, shown in white. Real trajectories will lie between these two extreme cases; if the escape forces are applied rapidly or slowly, the trajectory will be close to one of these extreme cases.

#246249 Received 21 Jul 2015; revised 28 Aug 2015; accepted 30 Aug 2015; published 8 Sep 2015

objects [15]. If the surface of the coverslip or slide is close enough to matter, the increase in viscous drag can be calculated using Faxén's correction [18] or the exact solution [19].

Due to the linearity of the equations describing fluid flow and forces resulting therefrom at very low Reynolds numbers, viscous drag resisting motion due to the optical force can be treated separately from the viscous drag applied by acclerating motion of the stage (the escape force). The escape force is

$$\mathbf{f}_{\mathrm{esc}} = \Gamma\mathbf{V} = 6\pi\eta r\mathbf{V} = 6\pi\eta rt\mathbf{a}, \tag{4}$$

where $\mathbf{V}$ is the stage velocity when the particle escapes the trap, $\mathbf{a}$ is the acceleration of the stage. Here, we assume that the stage is at rest until $t = 0$, when it begins to move with constant acceleration. For $t < 0$, $\mathbf{f}_{\mathrm{flow}} = 0$, and afterwards, the flow force increases over time independent of space.

The optical force is a function of position, and is calculated using generalized Lorenz–Mie theory with our Optical Tweezers Toolbox [20]. We also include the weight $\mathbf{f}_{\mathrm{w}}$ and buoyancy $\mathbf{f}_{\mathrm{b}}$ of the particle as forces; these are independent of time and position.

Simulations are performed using discrete time steps, with the forces calculated at step i, corresponding to time $t = t_i$, as a function of the current position $\mathbf{x}_i$ and particle and stage velocities $\mathbf{v}_i$ and $\mathbf{V}_i$. The position of the particle at the next step, $i+1$, is found using Euler's method:

$$\mathbf{x}_{i+1} = \mathbf{x}_i + \Gamma^{-1}\left(\mathbf{f}_{\mathrm{flow}}(t_i) + \mathbf{f}_o(\mathbf{x}_i) + \mathbf{f}_{\mathrm{w}} + \mathbf{f}_{\mathrm{b}}\right)\Delta t, \tag{5}$$

where $\Delta t = t_{i+1} - t_i$.

It is straightforward to include Brownian motion, as a random spatial motion, with probability distribution dependent of the duration of the time step, Δt [16]. Since we are simulating the escape of relatively large spheres, Brownian motion will not substantially affect the simulations. After trial calculations to confirm that Brownian motion could be ignored, simulations were performed without including it.

The particle position and velocity and the optical force were recorded for each time step during the simulation. The experimental escape force calibration used a camera to recored the position of the particle, and found the escape fluid velocity and force from these position measurements. Similarly, the particle position in the simulation was used to find a simulated escape force. The escape force was then compared with the actual optical forces during the escape.

3. Experiments

Experimental measurements were performed in two different laboratories. In the laboratory at Brisbane, Queensland, Australia, the experiment was performed with an optical tweezers setup using a computer-controlled piezo-electric stage (PI-563.3CD, Physik Instrumente) operating in closed-loop mode and controlled with a PCI card (PI-751E, Physik Instrumente). The trapping laser was a power and polarisation-stabilised ytterbium-doped fibre laser (YLM-5-LP, IPG Photonics) with output wavelength of 1070 nm, which underfills a numerical aperture NA = 1.3 microscope objective (Zeiss Plan Fluor EC100) to trap 4.5 μm diameter polystyrene spheres (Polysciences Pty. Ltd.). The method consisted of accelerating the stage at a constant rate until the sphere escaped the optical trap at a radiant laser power estimated at about 10 mW at the focus. Due to the underfilling of the objective, the convergence of the beam was that of a beam optimally filling (i.e., truncated where the irradiance falls to $1/\mathrm{e}^2$ of the central irradiance of the Gaussian profile) an objective with NA $\simeq 1.0$. The results from this investigation are shown along with simulations in Fig. 3.

The optical tweezers experiment at Irvine, CA, USA, has been described in [10]. The trapping laser was a 1064 nm ytterbium fiber laser (PYL-20M, IPG Photonics), focussed by a

#246249 Received 21 Jul 2015; revised 28 Aug 2015; accepted 30 Aug 2015; published 8 Sep 2015

high numerical aperture (NA = 1.4) oil immersion, Phase III, 100× objective (Zeiss Plan-Apochromat). Since trapping was performed far from the coverslip, the trap was affected by aberrations, and comparison of simulations and experimental measurements showed that the trap could be modelled as a trap produced by focussing the beam with an objective of NA = 0.8, without aberrations. A microstepper-motor driven stage for inverted microscopes (Ludl Electronic Products, BioPrecision2, NY, USA) was used to move the stage, controlled by the LabView (LabView 8.5.1, National Instruments, TX, USA) based RoboLase III system software [21]. The method consisted of accelerating the stage at a constant rate until the sphere escaped the optical trap. Sets of experiments were run for 4.5 μm and 10 μm diameter polystyrene spheres in methyl cellulose solution with viscosities of 1, 3 and 7 cP, with stage acceleration of 1×10^{-6}ms^{-2} and radiant laser power of 25–60 mW.

On both sets of apparatus, the trapping beam is propagating upwards, and the fluid flow produced by movement of the stage is horizontal. Position measurements of particles are performed using a camera imaging the particle, with image analysis providing the coordinates of the center of the particle for each frame.

4. Results and discussion

The position and velocity resulting from a simulation of a plausible escape scenario are shown in Fig. 3. As the drag force due to the motion of the stage increases as the stage accelerates, the displacement of the particle from the beam axis (i.e., the radial equilibrium position of the trap) slowly increases. When the particle escapes from the trap its velocity transitions to match the velocity of the surrounding fluid (i.e., the stage velocity). The change of velocity from the trapped to free floating regime can be used to determine the time of escape. The stage velocity at the time of the escape nominally gives the drag force at the time of escape, which should be approximately equal to the escape force.

In Fig. 4, we show trajectories of a 4.5 μm diameter polystyrene sphere as it escapes from a 5 mW trap. The optical force in the a) axial (z) and b) radial (x) directions is shown in the background. Each trajectory corresponds to a different stage acceleration. For low accelerations, the trajectory is close to the zero axial force contour. For high accelerations, the escape trajectory is closer that of the direction of the applied drag. The optical forces experienced by the particle along each trajectory are different due to the time it takes for the particle to reach dynamic equilibrium with the changing forces.

If we compare the forces encountered along the escape trajectory with the radial force–position curve (Fig. 5), we can see how lower accelerations reduce the maximum radial optical force that can be exerted by the trap [13, 14]. As the acceleration increases, the optical force during the escape approaches the straight-line radial force–position curve.

Figure 6 shows the transition between the high acceleration, high escape force regime, and the low acceleration, low escape force regime. For the smaller particles considered (diameter of 4.5 μm), the transition is similar for different powers. For the larger particles (diameter of 10 μm), the curves for the escape force efficiency differ by much more. As a result, even if escape force measurements for different powers are all performed in the low acceleration regime, the escape force efficiency will depend on the power. This slight power dependence can be seen in the experimental measurements shown in Fig. 7.

Since the maximum radial forces depend on the stage acceleration, different accelerations lead to different measurements of the escape force efficiency Q_{esc}. In Fig. 6, we scale the results by the ratio of the square of the power to the acceleration, which implies a constant of proportionality between the external force, optical force and the escape trajectory. However, due to the time it takes the particle to reach dynamic equilibrium the power normalised curves qualitatively match but do not coincide. For larger particles dynamic equilibrium is reached

#246249 Received 21 Jul 2015; revised 28 Aug 2015; accepted 30 Aug 2015; published 8 Sep 2015

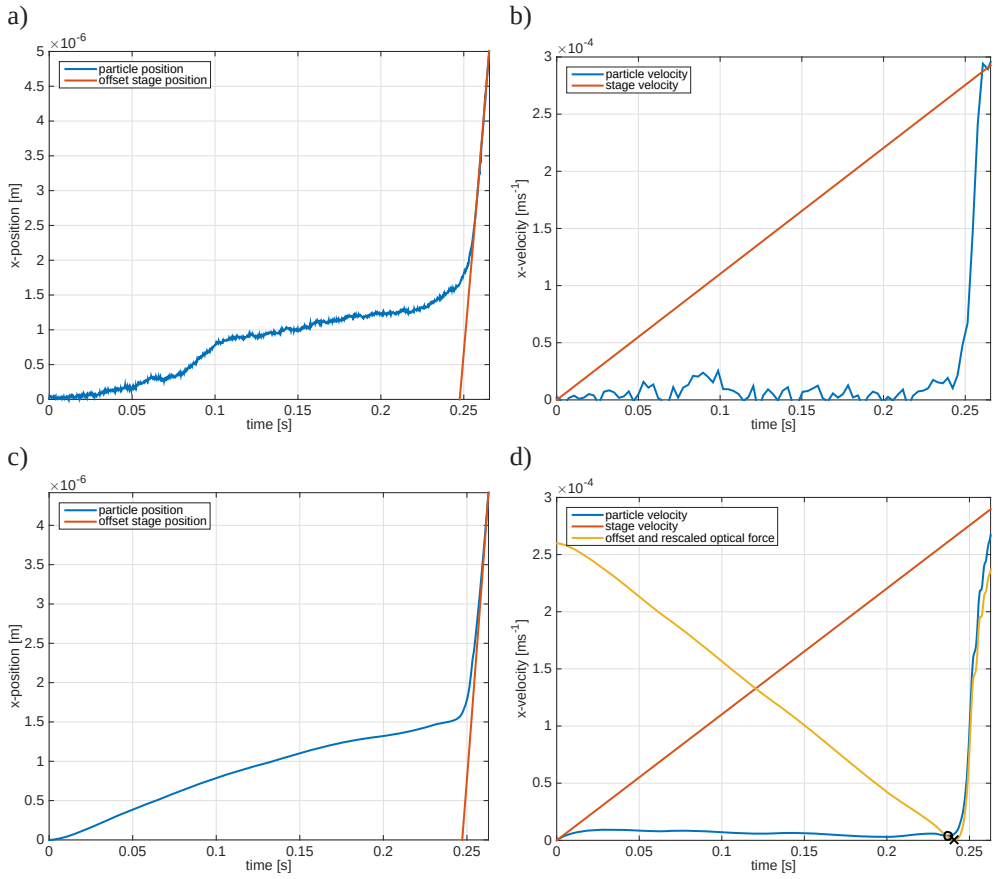

Fig. 3. Experiment and simulation of escape of a 4.5 μm diameter polystyrene sphere, trapped by 10 mW 1070 nm laser beam focussed by a numerical aperture NA = 1.3 objective. a) Position of particle. The stage position is shown with an offset so that the stage and particle are shown at the same position after escape. b) Averaged velocity of particle over 15 data points. As the stage velocity is increased the the particle will be displaced from the trap by the viscous drag force. The particle escapes around the point the particle velocity changes behaviour such that it begins to approach the fluid velocity. The particle moves rapidly away from the trap, at the velocity of the surrounding fluid (i.e., the stage velocity). c) Simulated position. d) Simulated velocity. Due to the lag introduced by dynamics, the maximum optical trap force ($\times$) is not coincident with the local minimum velocity prior to escape ($\circ$). Thus one cannot exactly know what the escape force is using only the particle position data.

even more slowly and thus the overlap is degraded further, thus there is a variation with power in the measured Q_{esc} even if all measurements are in the low acceleration regime.

Further variation is provided by the effect of weight and buoyancy. The zero axial force surface in the trap is where the total axial force, which includes weight and buoyancy, is zero. While the optical forces will change when the power changes, the weight and buoyancy will not, and the zero axial force surface will shift. Therefore, the escape trajectories will differ, and different escape forces can result. For low powers and large particles, this variation in the

#246249 Received 21 Jul 2015; revised 28 Aug 2015; accepted 30 Aug 2015; published 8 Sep 2015

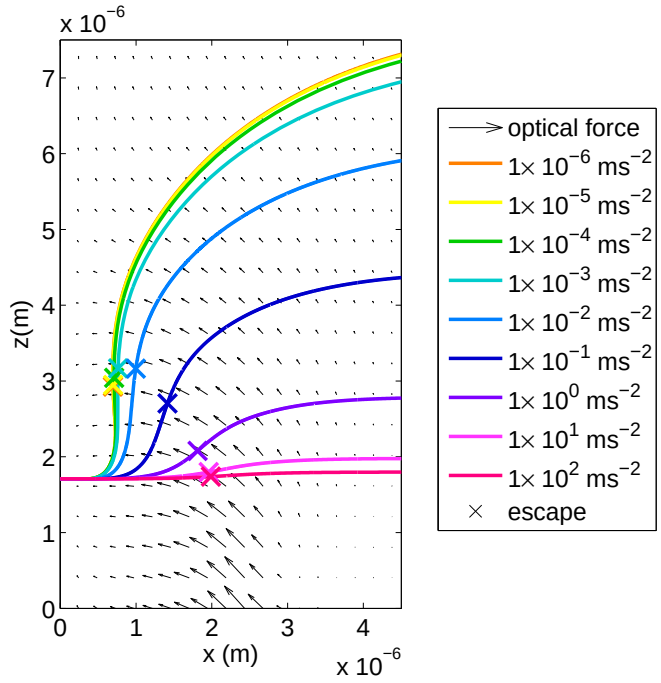

Fig. 4. Simulation showing the optical force field and the escape trajectories of a 4.5 μm diameter polystyrene sphere as it escapes from a 5 mW trap in water. Escape trajectories are shown for different stage accelerations. For low accelerations, the trajectory lies close to the zero axial force contour, and for high accelerations, it lies close to a straight horizontal line. The crosses mark the peak force, escape force, which correspond to the point of escape for each of the trajectories. The low acceleration particles escape by overcoming the axial trapping force, rather than the radial (x) trapping force. As the particle moves away from the beam axis, it moves upwards. At the radius where escape occurs, the particle ceases to be axially trapped. For high accelerations, escape occurs when the fluid flow force exceeds the maximum radial force encountered along the trajectory. These escapes of the particles along the different trajectories leads to different escape forces, as can be read from the x-force strength at the point of escape marked by the cross. Note that the sign of this radial force is negative as it points towards the centre of the trap, which is in the negative direction. The zero on the coordinates refers to the position of the focus: the equilibrium trapping position, before applying external fluid flow force, being beyond the focus.

#246249 Received 21 Jul 2015; revised 28 Aug 2015; accepted 30 Aug 2015; published 8 Sep 2015

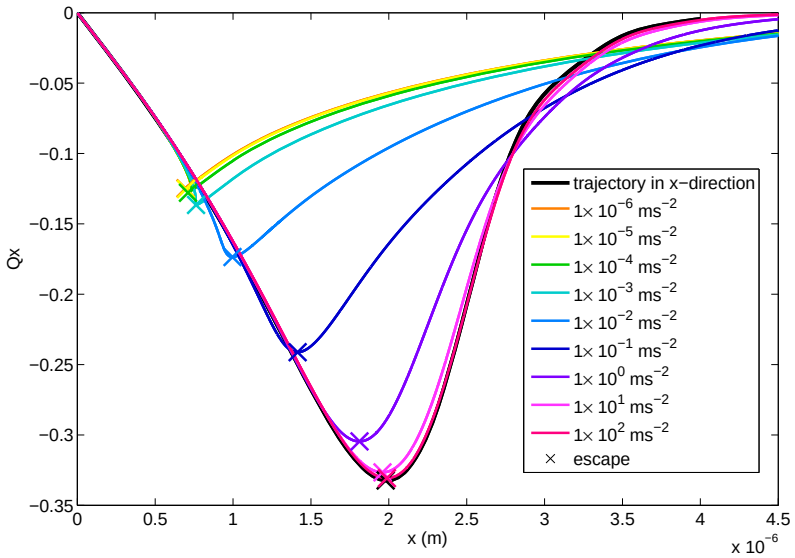

Fig. 5. Simulation showing optical force during escape. The radial normalised optical force efficiency, Q_x, encountered during the escape is shown for a range of stage accelerations, that is, over a range of rates of applying the external fluid flow force, which correspond to the escape trajectories shown in Fig. 4. This is compared to the force acting on the particle which has an escape trajectory directly out of the trap in the x-direction. The low acceleration trajectories have lower maximum radial forces than if the particle was to go directly in the x-direction. This trap and particle are the same as for Fig. 4.

zero axial force surface can be large. The effect of weight and buoyancy on the escape trajectories, and the radial forces during escape, are shown in Fig. 8, for 10 μm diameter polystyrene spheres trapped in water by a 5 mW 1064 nm laser beam focussed by a numerical aperture NA $= 0.8$ objective. For this particle and power, the effect of weight and buoyancy can produce a difference of 17% in the escape force efficiency in the low acceleration regime, and 6% in the high acceleration regime, comparing an upward-propagating trap with weight opposing the axial scattering force with a trap neglecting the effect of weight and buoyancy.

This provides a good explanation for the variation in Q_{esc} seen in [10]. The larger a particle is, the more drag ($\propto r$) and less optical trap stiffness ($\propto 1/r$) it experiences, and the more influence weight and buoyancy have ($\propto r^3$), creating a situation where variations between trajectories for different powers due to time taken to approach equilibrium are roughly proportional to r^2, and variations due to weight are roughly proportional to r^4. The simulations and corresponding experimental measurements of escape force have variations characteristic to following the zero axial force surface. These measurements are shown in Fig. 7. Deviations between the two are due to difficulty in precisely determining all the parameters to incorporate into the simulation.

Some of our data shown in Figs. 6 and 7 have been previously published [10, 11]. Here we include some of these data along with the new data for the purposes of clarity and to add context to our conclusion.

#246249 Received 21 Jul 2015; revised 28 Aug 2015; accepted 30 Aug 2015; published 8 Sep 2015

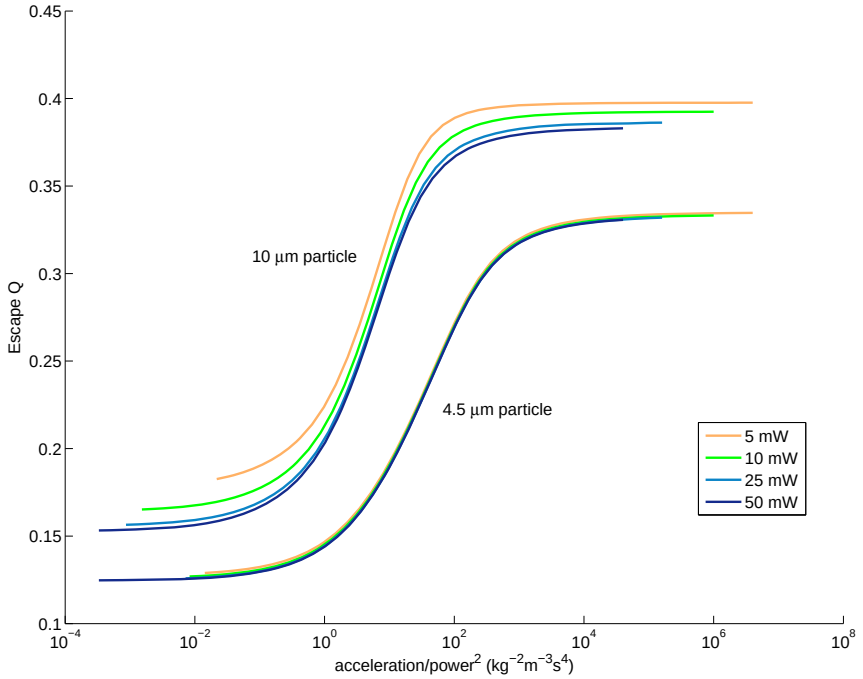

Fig. 6. Simulation showing the transition from low acceleration, low Q_{esc} region to high acceleration, high Q_{esc} region, for 4.5 μm and 10 μm diameter polystyrene spheres trapped in water by a 1064 nm laser beam focussed by a numerical aperture NA = 0.8 objective. The curves for different trapping powers do not overlap, and this non-overlap is larger for larger particles. This results in variations in Q_{esc} even if all measurements are in the low (or high) Q_{esc} regime.

5. Conclusion

We have shown that consistent with [13, 14] the variation of escape trajectories with stage acceleration and/or trapping power can result in variation of escape force efficiency Q_{esc} of up to a factor of two. Calibration by determining the spring constant at the equilibrium position is not even approximately accurate for escape force estimates, nor is it sufficient to calibrate the forces in a static external force field if practical measurements involve time dependent external forces. We have shown that in principle it is possible to account for the variation of escape force in time dependent external field, but this requires a sufficiently detailed knowledge of the optical potential. In order to avoid very large errors, it is important to consider whether the low acceleration, low Q_{esc} regime, or the high acceleration, high Q_{esc} regime is appropriate for calibration. This is not only a matter of considering the rate at which an increasing force is applied to trapped particles to produce escape, but also a matter of the vertical mobility of the particle. If, for example, adhesion forces between the trapped particle and a surface are being measured, the particle might not be free to move vertically to follow the zero axial force surface, even if the rate at which the force is increased is very low. In this case, the high acceleration regime will be more appropriate. Even if the calibration and force measurements are all performed in the low acceleration, low Q_{esc} regime (or the high acceleration, high Q_{esc}

#246249 Received 21 Jul 2015; revised 28 Aug 2015; accepted 30 Aug 2015; published 8 Sep 2015

a)

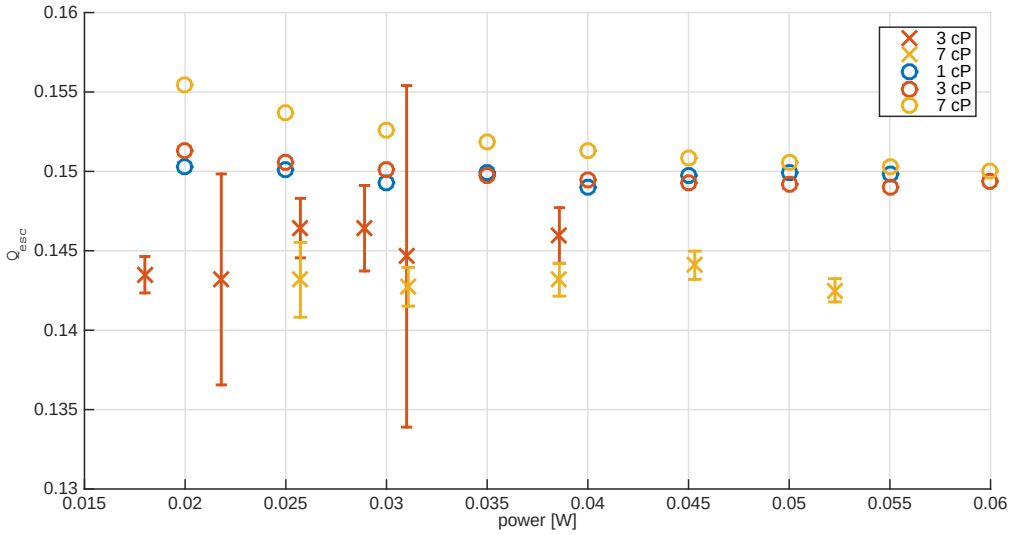

b)

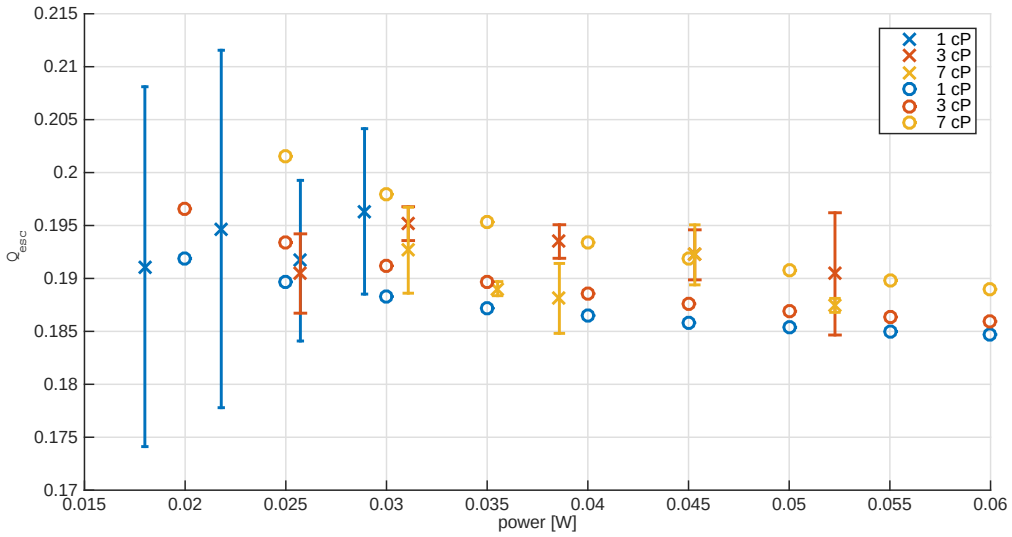

Fig. 7. Comparison of simulated (circles, ○) and experimental (crosses, ×) escape force (Q_{esc}) for a) $4.5\mu m$ and b) $10\mu m$ diameter polystyrene particles in methyl cellulose solution with viscosities of 1 cP, 3 cP and 7 cP.

#246249 Received 21 Jul 2015; revised 28 Aug 2015; accepted 30 Aug 2015; published 8 Sep 2015

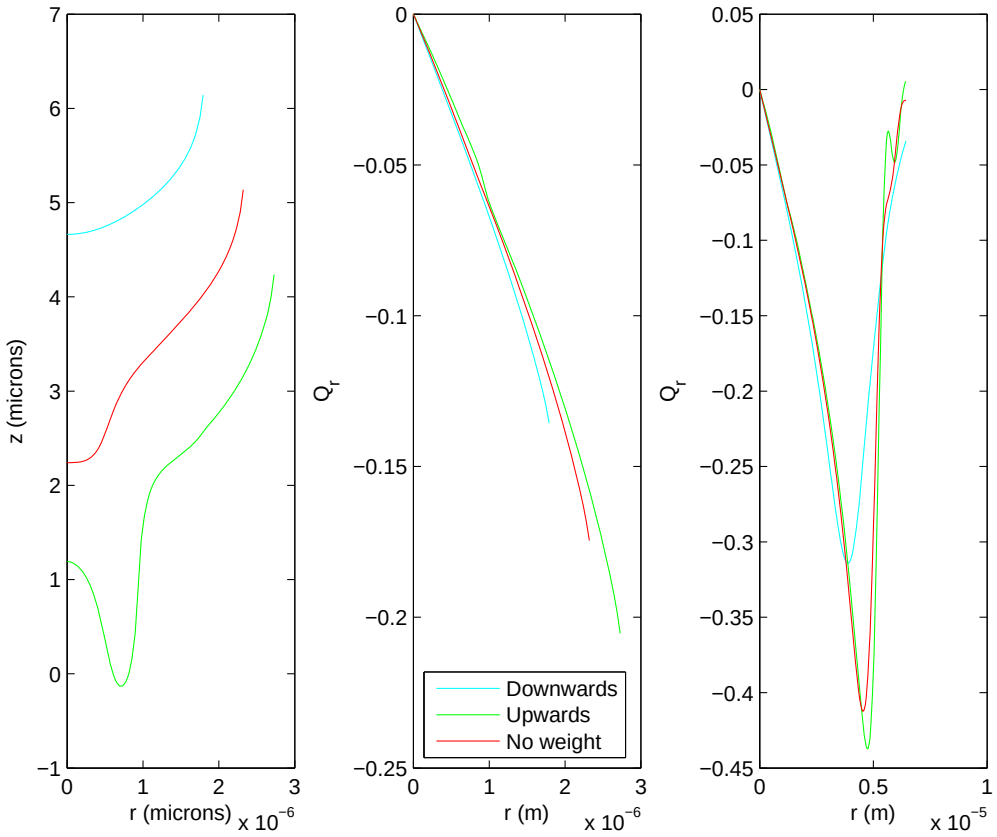

Fig. 8. Effect of weight and buoyancy on escape trajectories and forces for 10 μm diameter polystyrene spheres trapped in water by a 5 mW 1064 nm laser beam focussed by a numerical aperture NA = 0.8 objective. Three cases are shown: an upward-propagating trap where the weight opposes the axial scattering force, a downward-propagating trap where the weight acts in the same direction as the axial scattering force, and a trap with zero weight and buoyancy. As the power increases, the zero axial force surface will approach this zero weight and buoyancy case. (a) Zero axial force surfaces. These are the trajectories for escape with very low accelerations. For very high accelerations, the trajectories will be straight horizontal lines, with heights depending on the weight and buoyancy. (b) Radial force for very low accelerations. (c) Radial force for very high accelerations.

#246249 Received 21 Jul 2015; revised 28 Aug 2015; accepted 30 Aug 2015; published 8 Sep 2015

regime), variation of 20% or more in Q_{esc} can still occur.

At the very least, the physical effects we have explored need to be considered when estimating the experimental uncertainty in force measurements involving dynamic external forces. If the resulting uncertainty would be undesirably large, steps can be taken to mitigate this. Some possibilities are:

1. Observe the acceleration encountered during the escape, and perform a post-measurement calibration with this acceleration.

2. Observe the height of the particle at escape, and, from escape calibration at different accelerations (and therefore escape heights) and/or computational modelling, use the appropriate escape height dependent Q_{esc} to determine the escape force.

3. Since the main variation in escape force is due to the different radial distances that the particle can escape at—the force–position curves shown in Fig. 5 are similar before escape occurs—the escape force can be estimated with reasonable accuracy from the radial position at escape. The force–position curve can be measured using an escape at the highest available acceleration, from the variation of position with time.

4. Direct, but approximate, measurement of the optical forces during the escape using a calibrated position sensitive detector (PSD) or some other detector such as a camera [22]. This can be unreliable for large or high-refractive index [22] particle force measurements due to the reliance on the complete collection of scattered light, and aberrations or nearby surfaces can interfere with such optical force measurements.

We have demonstrated important effects and strategies not commonly considered in optical tweezers experiments. Consideration of these effects and strategies may explain a number of inconsistencies observed in experiments involving the escape from or near the limit of an optical trap.

Acknowledgments

This research was supported under Australian Research Council's Discovery Projects funding scheme (project number DP140100753).

#246249 Received 21 Jul 2015; revised 28 Aug 2015; accepted 30 Aug 2015; published 8 Sep 2015